# Supplemental Information

## Clustering and functional coupling of diverse ion channels and signaling proteins revealed by super-resolution STORM microscopy in neurons

**Authors:** Jie Zhang, Chase M. Carver, Frank S. Choveau and Mark S. Shapiro*

Department of Physiology, University of Texas Health Science Center at San Antonio

*Correspondence to: shapirom@uthscsa.edu

## Inventory of Supplemental Information

**Supplemental Experimental Procedures**

**Primary neuron culture**

Sympathetic and sensory neurons were isolated from the superior cervical ganglia (SCG) of 7-14 day old mice (C57BL/6) and cultured for 2-4 days. Mice were anesthetized with halothane and decapitated. Neurons were dissociated using established methods(Bernheim et al., 1991), plated on 4 x 4 mm glass coverslips or Lab-Tek$^{TM}$ II chambered coverglass (coated with poly-L-lysine) and incubated at 37ºC (5% $CO_2$). Fresh culture medium containing nerve growth factor (50 ng/ml) was added to the cells 3 hrs after plating.

**AKAP150 Transgenic mice**

We maintain a colony of AKAP150 (+/+) and (-/-) mice (C57BL/6 background) at UTHSCSA (originally supplied to us by Dr. G. Stanley McKnight, University of Washington; RRID:IMSR_JAX:026692). Mice were housed in groups of five and maintained under a 12:12 h light-dark cycle with food and water provided ad libitum. Mice were backcrossed (+/+ x -/- to yield +/-) every 6th generation. Genotype comparisons were made among littermates and mice were bred by intercross to produce all three genotypes within a litter. A small piece of tissue taken from the end of the tail (tail clip) was used to genotype the mice by real-time (quantitative)-PCR on an Applied Biosystems PRISM 7000 Real-Time PCR sequence detection system. The probe and detailed protocol for performing these analyses were also kindly provided by Drs. Stanley McKnight and Johannes Hell (University of California, Davis). The primers used for qRT-PCR for AKAP150 were 5'-GGCCTTGTGACACACAGGAA-3' and 5'-CAGGCGGCTTCTGCTTCTT-3' and the fluorescent probe is VIC-AGGTCCGAGCCTGC-MGBNFQ, and for Neo, the primers are 5'-ATGGCCGCTTTTCTGGATT-3' and 5'-GCCAAGCTCTTCAGCAATATCA-3', and the fluorescent probe is VIC-CGGACCGCTATCAGG-MGBNFQ. Samples were run through 40 cycles and each sample was run in duplicate for both AKAP150 and Neo. To minimize user bias, cycle thresholds (Ct) were calculated automatically using the Applied Biosystems software. As a control against Neo contamination, all of our littermate genotyping analyses included tail clips from two AKAP150 (+/+), two (+/-) and two (-/-) mice as control. Genotyping results were only accepted if the Ct values for both AKAP150 and Neo were not significantly different from controls.

**STORM methods and experiments to control for source of error**

Our super-resolution STORM method uses primary antibodies against proteins of interest, coupled to secondary antibodies conjugated in-house with activator-reporter dye pairs (Zhuang, 2009). The activator dyes (Alexa 405, Alexa 488 and Cy3) are stimulated with the appropriate laser lines, and the reporter dye (Alexa 647) is driven into the dark state or fluorescently excited by the 647 nm laser after selective non-radiative energy coupling by the activator dye, as demonstrated in *Supplemental Movie 1*. Although it is not precisely known how close the activator and reporter dyes must be for efficient energy coupling, it is surely within the 20 nm (200 Å) of our STORM resolution. Given the various sources of error inherent in such a method that entails enormous signal amplification and computer reconstruction, it was incumbent upon us to perform a number of control experiments to verify the reliability and veracity of our images (*see below*). We are satisfied that all the sources of error are minor, in relation to the signal.

In our STORM imaging, to insure that only a single fluorophore is imaged per cycle at any given location, strong laser illumination was used to photoswitch the vast majority of "reporter" fluorophores into a temporary dark state. A subset of the reporter fluorophores are then photoswitched into an active, excitable state by weak excitation of a conjugated fluorophore called the activator. Activated reporters were imaged for several frames (1 frame = 16 ms) until they were again switched into the dark state. A second or third subset of reporters was subsequently activated, and the cycle repeated over ~30 min (~10,000 cycles) to build up a super-resolution reconstruction. The N-STORM set-up we used achieves lateral and axial resolutions of ~10 nm and ~50 nm, respectively. Near-TIRF (oblique) illumination was employed using a CFI 100X/NA 1.49 oil immersion objective and an Andor iXon3 EMCCD camera. On the N-STORM Nikon system, the "oblique setting" we used was usually 3,000, which is an arbitrary unit. Nikon Elements software was used for both data collection and analysis. 405, 488, and 561 nm laser lines were used respectively for activation dyes, Alexa 405,

Alexa 488, and Cy3. Reporter dye, Cy5 or Alexa 647, was excited using a 647 nm laser line. The imaging protocol for multi-color, multi-protein localization consists of sequential activator/reporter cycles, using different activators excited by distinct laser lines that photo-activate the same reporter (in this case, A647). STORM molecule data acquisition involved each imaging cycle at one frame (16 ms) of activation laser (405 nm, 488 nm, or 561 nm) followed by three frames of imaging reporter laser (647 nm). Since only one set of reporters are activated, it is required that the software assign the brief emission (called a "blink") of a fluorophore to the correct protein, based on which activator dye is excited.

STORM imaging was performed in a freshly prepared imaging buffer that contained 50 mM Tris (pH 8.0), 10 mM NaCl and 10% (w/v) glucose, with an oxygen-scavenging GLOX solution (0.5 mg/ml glucose oxidase (Sigma-Aldrich), 40 μg/ml catalase (Sigma-Aldrich), and 10 mM cysteamine MEA (Sigma-Aldrich). MEA was prepared fresh as a 1 M stock solution in water, stored at 4°C and used within 1 month of preparation. Acquisitions were made from between 2-4 different experiments for labeling and imaging. Images were rendered as a 2D Gaussian fit of each localization. The diameter of each point is representative of the localization precision (larger diameter, less precise), as is intensity (more intense, more precise). Signal-noise thresholds were handled as peak height above the local background in the N-STORM software. A detected peak was set as the central pixel in a 5x5 pixel area, and the average intensity of the 4 corner pixels was subtracted from intensity of the central pixel. Using a 100x objective and 16 x 16 μm pixel are of the iXon3 camera, this corresponds to a 0.8 μm x 0.8 μm physical neighborhood. In order to demonstrate the incidence of protein clustering, rendered images were filtered to remove background localizations. The density filtering process was used based on two parameters supplied by the N-STORM software: *radius*, *max*, the maximum neighborhood search radius of localization rendering, and *count*, the minimum number of localizations to form a cluster. We used a density filter with *count* of 3-5 molecules and *radius* of 200 nm. The rationale for choosing these parameters was based on the observed clustering of signaling proteins, in which unfiltered, single localizations >200 nm were outside the range of nearest neighbor distances. Thus, points that did not meet density requirements were removed from the rendered image as background noise. We also empirically altered these parameters over a suitable range, but did not find a distinct parameter set that better quantified the cluster properties.

**Labeling of secondary antibodies with dye pairs.**

For our experiments, Alexa Fluor647 carboxylic acid (Invitrogen, #A20006) was utilized as the photo-switchable reporter fluorophore (Dempsey et al., 2011). The activator dyes used were Alexa Fluor405 carboxylic acid (Invitrogen, #A30000), Alexa Fluor488 carboxylic acid (Invitrogen, #A20000), Cy2 bis-reactive dye pack (GE Healthcare, #PA22000), Cy3 mono-reactive dye pack (GE Healthcare, #PA23001). Unconjugated secondary antibodies were obtained from Jackson Immunoresearch Laboratories, including AffiniPure or AffiniPure F(ab')$_2$ Fragment of Donkey Anti-Mouse IgG (H+L) (Jackson ImmunoResearch Labs Cat# 715-007-003, RRID:AB_2307338), Donkey Anti-Rabbit IgG (H+L) (Jackson ImmunoResearch Labs Cat# 711-005-152, RRID:AB_2340585), Donkey Anti-Goat IgG (H+L) (Jackson ImmunoResearch Labs Cat# 705-005-003, RRID:AB_2340384), Donkey Anti-Guinea Pig IgG (H+L) (Jackson ImmunoResearch Labs Cat# 706-005-148, RRID:AB_2340443). To label secondary antibodies with an activator-Alexa Fluor647 pair, activator and reporter dyes were dissolved in DMSO. Secondary antibody (50μl) was mixed with 1.5 μl Cy3 (or 4 μl Alexa Fluor405, or 5 μl Cy2), 0.6 μl Alexa Fluor647 and 6 μl of 1M $NaHCO_3$, incubated for 30 min, and then run through NAP-5 columns (GE Healthcare, #17-0853-02). Eluents were collected and absorbance of labeled secondary antibody was measured on UV/visible wavelength spectrophotometer. The labeling ratio was calculated by concentration of the antibody, activator and reporter dyes using Beer-Lambert's law. Antibodies with a labeling ratio of activator dye: antibody:reporter dye =2.0-3.0: 1:0.6-1 were used in our STORM experiments.

In our STORM imaging, we considered a number of sources of potential artifacts, which can arise from *1) Crosstalk,* or "non-specific activation" automatically detected in the N-STORM software (Elements, Nikon) which refers to the subpopulation of reporter dye molecules that become activated or remain activated after the first reporter frame, independent of the activator laser. This is because reporter dyes can blink stochastically at some low basal rate (regardless of how long ago the last activation pulse was); *2) Excitation spectral overlap*, which is the traditional excitation spectral overlap of the activator dye pairs among activator laser lines; *3)*

*Direct non-specific excitation*, which is the direct activation of reporter dye molecules by the activator laser lines, and *4) Cross activation*, which is the activation of the reporter dye molecules on closely nearby proteins by the other non-co-conjugated activator dyes.

The N-STORM analysis module of the NIS-Element software recognizes molecules belonging to **#1** and assigned a probability to each molecule based on its neighbors. If the neighborhood was judged to be specific (*i.e.*, few appearing in the 2nd and 3rd frames), the molecule in question is probably specific. If dye molecules are not co-localized, this is a reasonable assumption. "Crosstalk subtraction" in the analysis module was used as a statistical method to remove molecules by comparing their assigned probability to a random number. Each cycle, after the activator laser excites the photo-switchable dye pair during the initial frame, only molecules detected in the first imaging frame after activation are classified as corresponding to the proper activation wavelength and channel. Subsequent imaging frames are classified as from non-specific activation and discarded. As previously described (Dani et al., 2010), the probability of non-specific activation events by the imaging laser should be consistent across frames with or without a preceding activation laser frame. Therefore, the total numbers of specific and non-specific activation events across all imaging cycles were used to statistically subtract crosstalk. For each channel and localization, the local density of the total number activated molecules ($n_A$) and the number of specific activation events ($N_A$) was determined based on a normally distributed proximity distance to the localization. The localization was removed with a probability of $P = (n_A - N_A)/n_A$. Therefore, if there were fewer reporter molecules appearing in the 2nd and 3rd imaging frames proximal to that localization, the localization in question was more likely to be specific. Since the acceptance/rejection threshold is a judgment call based on a slider set by the user, for an unbiased subtraction across experiments, we selected the random subtraction option by the N-STORM system. We are aware of the possible minor error from *#1* if proteins are co-localized, which can be avoided using "D-STORM" in the future because even if molecules come out of the dark state at the wrong time, the laser that causes them to fluoresce will not be on.

We performed sham triple-color STORM with each of the three activator lasers turned off (405 nm 0%, 488 nm 0%, 563 nm 0%, and 647 nm 100%) on triple-labeled CHO cells transfected with KCNQ2, AKAP150 and KCNQ3. The localizations for each channel collected in this control were ~2%, 2% and 2% of those when the respective lasers were turned on. **Error #2** is only a concern when using Alexa 488 and Cy3 activators, as the absorbance spectra of those two dyes do have modest overlap. This was handled and corrected mathematically based on activation laser energy by the NIS-Elements software in the analysis module. We are aware of the possible "direct non-specific excitation" of **Error #3**, plus the possible minor error from **Error #1** if proteins are co-localized; thus we calculated these errors by performing triple-color STORM with three activator lasers turned on (405 nm 0.5%, 488 nm 2%, 563 nm 0.5%, and 647 nm 100%) on singly labeled CHO cells. When CHO cells were transfected with KCNQ2 and labeled with Alexa 405/Alexa 647 only, the normalized molecule numbers for each channel we collected were 100%, 6.6% and 3.8%. When CHO cells were transfected with TRPV1 channels and labeled with Alexa 488/Alexa 647 only, the normalized molecule values were 7.9%, 100% and 9.7%. When CHO cells were transfected with KCNQ2 and labeled with Cy3/Alexa 647 only, these values were 11.2%, 10.1% and 100%. Possible cross-activation from **Error #4** is not worrisome to us because it can only occur if the two proteins are in intimate association, which is the goal of our STORM imaging. Thus, the overall sources of crosstalk in our STORM approach are well controlled.

**Antibodies.**

We purchased primary antibodies of rabbit anti-$M_1$ receptor (Millipore Cat# AB5164-50UL, RRID:AB_91713), goat anti-AKAP150 (Santa Cruz Biotechnology Cat# sc-6446, RRID:AB_2225903), mouse anti-$B_2$ receptor (BD Biosciences Cat# 610452, RRID:AB_397826), mouse anti-Myc tag to label myc-tagged KCNQ1 or KCNQ4 (Abcam Cat# ab17356, RRID:AB_2148459), mouse anti-Flag tag to label Flag-tagged $M_1$ receptor (Sigma-Aldrich Cat# F3165, RRID:AB_259529), and guinea-pig anti-TRPV1 (Neuromics Cat# GP14100, RRID:AB_2620140). Our rabbit anti-KCNQ2 (RRID:AB_2314688) and guinea-pig anti-KCNQ3 (RRID:AB_2314689) antibodies were given to us by Edward Cooper (Baylor College of Medicine), and the rabbit anti-$Ca_V1.2$ antibody was given to us by Johannes Hell (University of California at Davis; Davare et al., 1999, 2000). Antibody specificities for $M_1$ receptor, $B_2$ receptor, and AKAP150 were tested by neuronal immunochemistry in respective germline knockout mice. $Ca_v1.2$ and TRPV1 antibody validation and specificity

were confirmed via cDNA transfection in CHO cells followed by immunostaining. Samples that were not stained with primary antibody but exposed to secondary antibody were examined as non-antigenic controls in validation as well.

**cDNA constructs.**

Human KCNQ1-5 (Genbank accessions NM000218, AF110020, AF091247, AF105202 and AF249278, respectively) were kindly given to us by Michael Sanguinetti (KCNQ1, University of Utah, Salt Lake City, UT), David McKinnon (KCNQ2 (isoform *d*), SUNY, Stony Brook, N.Y.), Thomas Jentsch (KCNQ3, KCNQ4 (isoform *a*), Zentrum fur Molekulare Neurobiologie, Hamburg, Germany) and Klaus Steinmeyer (KCNQ5, Aventis Pharma, Frankfurt am Main, Germany). The plasmids for AKAP79, GFP-tagged AKAP79, AKAP150 were kindly given to us by Mark Dell'Acqua (University of Colorado Medical School, Aurora, CO). The plasmids for TRPV1 was kindly given to us by Nathaniel A. Jeske (University of Texas Health Science Center at San Antonio, TX).

**Reagents.**

TTX, NGF, bradykinin, capsaicin, nifedipine, thapsigargin and collagenase type I (Sigma); DMEM, fetal bovine serum, pennicillin/streptomycin (Gibco); amphotericin B (Calbiochem); XE991 (Tocris Bioscience). Items and sources of reagents used for STORM are detailed above.

**Nearest-neighbor distance analysis of STORM images.**

Molecules lists of three activator/reporter dye pairs (Alexa 405/Alexa 647, Alexa 488/Alexa 647, and Cy3/Alexa 647) from STORM images were exported from the N-STORM module of NIS-Elements in three separate *.txt* files, which contain corrected "X", "Y", and "Z" coordinates for each channel (color). The "X" and "Y" coordinates of these molecules was used as their precise locations in the images, and was input into a Matlab program to calculate the distances of each molecule with the other molecules from the same channel, or from the other channel(s). For each molecule, only the shortest distances in three channels (Alexa 405/Alexa 647, 488/Alexa 647, and cy3/Alexa 647) were saved, and these shortest distances were outputted in separate *.txt* files, which contain the shortest distances for the following pairs: Alexa 405 to Alexa 405, Alexa 405 to Alexa 488, Alexa 405 to Cy3, Alexa 488 to Alexa 488, Alexa 488 to Alexa 405, Alexa 488 to Cy3, Cy3 to Cy3, Cy3 to Alexa 405 and Cy3 to Alexa 488. Origin Pro 8 were used to plot the distances from each *.txt* file into distribution histograms with bin size of 10 nm, which were then fit with single- or double-Gaussian distribution.

To quantify the "lateral localization accuracy," we used Thompson's method (Thompson et al., 2002) as used by the Zhuang and colleagues in describing the STORM technique (Rust et al., 2006). The precision is based on the number of photons collected, which is calculated by our software based on the CCD characteristics provided by Andor, the camera settings used during acquisition (e.g., gain), and the recorded pixel intensity (grayscale values/"ADU's"). The lateral localization accuracies are reported for each dataset in Supplemental Tables S1, S2, S3, and S4, and are consistent with previously determined values using similar STORM acquisition techniques (Barna et al., 2016).

**Cluster size and localization proximity analysis**

Unfiltered STORM localization data were exported as molecular list *.txt* files from Elements and were analyzed with in-house software incorporating a density-based spatial clustering algorithm with noise (DBSCAN) (Ester et al., 1996). DBSCAN was used due to its insensitivity to the ordering of the points in the dataset, the lack of requirement for specifying the number of clusters *a priori*, in contrast to partitioning algorithms such as Ripley's K function, as well as a larger maximum number of detectable localizations per cluster (Rubin-Delanchy et al., 2015). A dense region or cluster was defined as localizations within a directly-reachable radius proximity (*epsilon*) from a criterion minimum number of other core localizations (*minimum points*). Density-reachable points were localizations that were within the epsilon radius of a single core point and thus considered part of the cluster. Localizations considered to be noise were points that were not within the epsilon distance of any core points of a cluster. We derived the appropriate epsilon parameter using the nearest-neighbor plot from single-dye labeled controls; cluster detection was determined for epsilon between 20 and 80 nm, which were the nearest-neighbor localization distances representing 95% of area under the curve. DBSCAN

parameters were verified by measuring *goodness of fit* to Gaussian distribution with cluster population data from single-dye labeled controls, and set for the distance of directly reachable points at 50 nm (epsilon) and 5 minimum points.

For cluster detection, each localization was assessed based on its corrected X and corrected Y 2D spatial coordinates, and the associated activator dye was tracked throughout analysis. Detected clusters were tabulated by the composition and number of resident activator dyes contributing to the total neighborhood of localizations for that cluster. Clusters were categorized based on activator dye composition as Alexa 405 only, Alexa 488 only, Cy3 only, Alexa405 + Alexa488, Alexa 405 + Cy3, or Alexa 405 + Alexa 488 + Cy3, according to the dye conjugated to each antibody label. Cluster radius data were placed in probability distribution histograms with a bin size of 5 nm. Symmetrical clusters predominated in identification of cluster radius size. Based on the observation that a majority of cluster distributions displayed positive skew, distributions were fit by the generalized extreme value distribution function: $f(x) = e^{-(x-1+e^{\wedge}-x)}$. Cluster size values were reported as mean ± SEM. The β continuous scale parameter (which is unit-less) of each cluster distribution was derived from the mean value of the extreme distribution (Mean = μ + γβ, *γ:* 0.5772, Euler-Mascheroni constant) and was determined as a metric for "tailedness" of the cluster size distribution. In addition, the percentage of clusters belonging to a labeling category out of total clusters compared. The noise threshold of a cluster distribution was determined from double-labeled KCNQ2 and KCNQ4 STORM images, given the widely accepted notion that KCNQ2 and KCNQ4 do not form heteromers, and thus should not demonstrate co-localization. Therefore, it is unlikely that a cluster distribution under the noise threshold represents a significant population of clusters. Cumulative distribution functions of cluster categories were compared with the Kolmogorov-Smirnov test. Population statistics for each cluster category were derived from 4-7 cells per staining and imaging condition. We only performed cluster radius analysis for experiments in neurons, as we felt that the more artificial heterologous expression system in CHO cells, while useful for establishing which proteins co-assemble, is probably not the best system for quantifying and comparing cluster sizes.

**Perforated-patch electrophysiology.**

Pipettes were pulled from borosilicate glass capillaries (1B150F-4, World Precision Instruments, Florida, USA) using a Flaming/Brown micropipette puller P-97 (Sutter Instruments) and had resistances of 1-4 MΩ when filled with internal solution and measured in standard bath solution. Membrane current was measured with pipette and membrane capacitance cancellation, and sampled at 5 ms and filtered at 1 kHz by an EPC-9 amplifier, and PULSE software (HEKA/Instrutech, Port Washington, NY). In all experiments, the perforated-patch method of recording was used with amphotericin B (600 ng/ml) in the pipette (Rae et al., 1991). Amphotericin was prepared as a stock solution as 60 mg/ml in DMSO. In these experiments, the access resistance was typically 5-10 MΩ 5-10 minutes after seal formation. Cells were placed in a 500 μl perfusion chamber through which solution flowed at 1-2 ml/min. Inflow to the chamber was by gravity from several reservoirs, selectable by activation of solenoid valves (Warner Scientific). Bath solution exchange was essentially complete by <30 s. Experiments were performed at room temperature.

M currents in sensory cells were studied by holding the membrane potential at -25 mV and applying a 500-ms hyperpolarizing pulse to -60 mV every 5 s. M-current amplitude was measured at -60 mV from the decaying time course of the deactivating current sensitive to the M-channel specific blocker XE991 (Zaczek et al., 1998). TRPV1 currents were studied by holding the membrane potential at -60 mV and TRPV1-current amplitudes quantified in response to application of capsaisin. The external solution contained (mM): 150 NaCl, 5 KCl, 2 $CaCl_2$, 1 $MgCl_2$, 10 glucose, 10 HEPES, tetrodotoxin 500 nM, pH 7.4 with NaOH. The pipette solution for voltage-clamp experiments contained (mM): 150 KCl, 5 $MgCl_2$ and 10 HEPES to record $I_M$. Data are presented as mean ± SEM. Statistical tests were performed using ANOVA, paired t-test, or unpaired t-test, where appropriate.

**Supplemental Discussion**

The analysis of NG neurons double-labeled for $Ca_V1.2$ channels and AKAP150 (**Fig. 5F**) shows a great preponderance of the clusters to contain both proteins, and almost no unpaired AKAP150 molecules. On the other hand, the NG neurons double-labeled for TRPV1 channels and AKAP150 seem to show only about half

the TRPV1 molecules in complex with AKAP150, and a large number of *seemingly* "unpaired" AKAP150 molecules. But this initial impression would be false. Indeed, **Fig. 5F** strongly suggests that almost all of the "unpaired" AKAP150 molecules in **Fig. 5E** are not solitary at all, but in fact are in complex with $Ca_V1.2$ channels, which are unlabeled and thus, "dark," in these double-labeled cells (their cluster radii are smaller than those of the $Ca_V1.2$/AKAP150 complexes only because the anti-$Ca_V1.2$ antibodies and corresponding dye-labeled secondaries are not present). Thus, the yellow histogram in **Fig. 5F** must be the sum of AKAP150 in complex with only $Ca_V1.2$ channels (one or many more than one), and the complexes consisting of AKAP150 in complex with $Ca_V1.2$ *and* TRPV1 channels. Consistent with this interpretation, the cluster analysis of NG neurons triple-labeled for AKAP150, and $Ca_V1.2$ and TRPV1 channels (**Fig. 8C**) report almost half the complexes to contain all three proteins (**Table S4**). We suspect the reason that this percentage is not even higher is indicated by the number of clusters representing isolated AKAP150, which is negligible; *i.e.*, there are no more available AKAP150 molecules. This analysis reinforces the interpretation that neurons do not express copies of AKAP150 equal to the copies of its binding properties, leading to the inevitable "competition for AKAP150" that we suspect *itself* leads to dynamic re-organization of complex members, dependent on the state of the neuron.

From the imaging and functional data from neurons of AKAP150 KO mice, and the associated analysis of these data (**Figs. 7B, 8D & 9**), our working hypothesis is that the "mega-clusters" of AKAP150 with multiple numbers of $Ca_V1.2$ channels requires, or is at least greatly facilitated, by inclusion of at least one TRPV1 channel, perhaps acting as a kind of molecular "catalyst channel." It will be extremely interesting to perform such experiments in TRPV1 KO mice, to probe if there is such a "catalyst channel" in heart and smooth muscle, and to examine the arrangement in brain, where TRPV1 channels are rare, but AKAP150-binding NMDA receptors in spines are numerous (Gomez et al., 2002), as are L-type $Ca^{2+}$ channels, both being critical to synaptic plasticity. Since we show in this work the coupled gating of M and TRPV1 channels, and TRPV1 and $Ca_V1.2$ channels, it stands to reason that the gating of all three of these channels in these super- or mega-complexes could be coupled. Again, we suspect that in other excitable cells, in which AKAP79/150 orchestrates similar signaling complexes, other channels likely play the roles seen here for KCNQ and TRPV1 channels, such as those in heart, smooth muscle and brain, in all of which AKAP79/150 brings multiple signaling molecules into intimate proximity.

**Supplemental References**


Barna, L., Dudok, B., Miczan, V., Horvath, A., Laszlo, Z., and Katona, I. (2016) Correlated confocal and super-resolution imaging by VividSTORM. Nature Protocols 11, 163-183.

Bernheim, L., Beech, D.J., and Hille, B. (1991). A diffusible second messenger mediates one of the pathways coupling receptors to calcium channels in rat sympathetic neurons. Neuron 6, 859-867.

Dani, A., Huang, B., Bergan, J., Dulac, C., and Zhuang, X. (2010). Superresolution imaging of chemical synapses in the brain. Neuron 68, 843-856.

Dempsey, G.T., Vaughan, J.C., Chen, K.H., Bates, M., and Zhuang, X. (2011). Evaluation of fluorophores for optimal performance in localization-based super-resolution imaging. Nat Methods 8, 1027-1036.

Ester, M., Kriegel, H.P., Sander, J., Xu, X. (1996) A density-based algorithm for discovering clusters in large spatial databases with noise. In Proceedings of 2nd International Conference on Knowledge Discovery and Data Mining (KDD-96). 226-231.

Gomez, L.L., Alam, S., Smith, K.E., Horne, E., and Dell'Acqua, M.L. (2002). Regulation of A-kinase anchoring protein 79/150-cAMP-dependent protein kinase postsynaptic targeting by NMDA receptor activation of calcineurin and remodeling of dendritic actin. J Neurosci 22, 7027-7044.

Rae, J., Cooper, K., Gates, P., and Watsky, M. (1991). Low access resistance perforated patch recordings using amphotericin B. J Neurosci Methods 37, 15-26.

Rubin-Delancy, P., Burn, G.L., Griffié, J., Willliamson, D.J., Heard, N.A., Cope, A.P., Owen, D.M. (2015) Bayesian cluster identification in single-molecule localization microscopy data. Nat Mehtods 12, 1072-1076.

Rust, M.J., Bates, M., and Zhuang, X. (2006). Sub-diffraction-limit imaging by stochastic optical reconstruction microscopy (STORM). Nat Methods 3, 793-795.

Thompson, R.E., Larson, D.R., Webb, W.W. (2002) Precise nanometer localization analysis for individual fluroescent probes. Biophys J *82*, 2775-2783.

Zaczek, R., Chorvat, R.J., Saye, J.A., Pierdomenico, M.E., Maciag, C.M., Logue, A.R., Fisher, B.N., Rominger, D.H., and Earl, R.A. (1998). Two new potent neurotransmitter release enhancers, 10,10-bis(4-pyridinylmethyl)-9(10H)-anthracenone and 10,10-bis(2-fluoro-4- pyridinylmethyl)-9(10H)-anthracenone: comparison to linopirdine. J Pharmacol Exp Ther 285, 724-730.

Zhuang, X. (2009). Nano-imaging with Storm. Nat Photonics 3, 365-367.

**Supplemental Figures.**

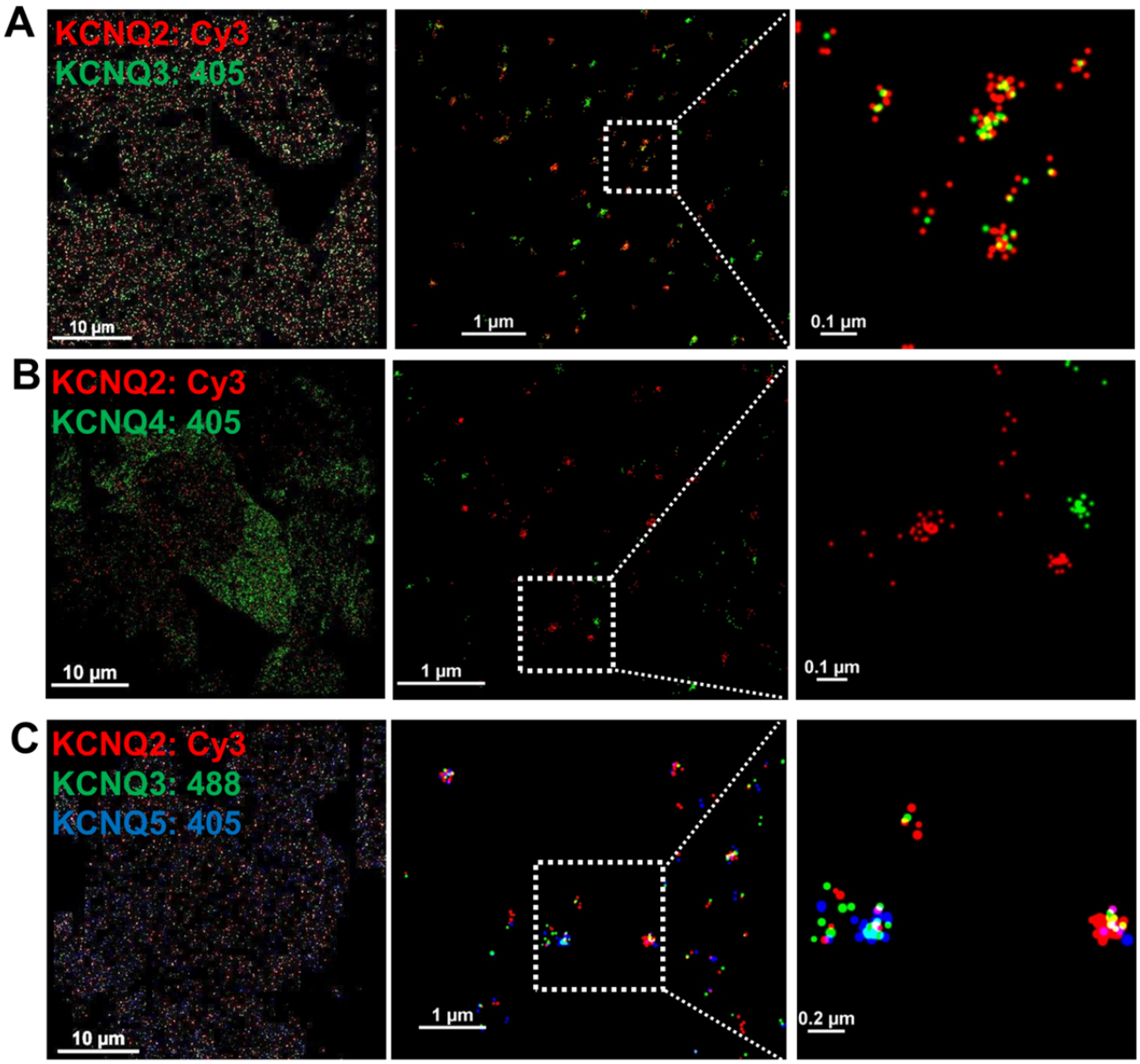


**Figure S1. Related to Figure 1. STORM microscopy distinguishes proteins that are intimately associated, from proteins that are not.**
For CHO cells co-transfected with KCNQ2+KCNQ3 **(A)**, KCNQ2+myc-tagged KCNQ4 **(B)**, or with KCNQ2+KCNQ3+myc-tagged KCNQ5 **(C)** at low density, raw STORM images before filtering the isolated, individual centroids are shown. n= 5, 4 and 5 cells.

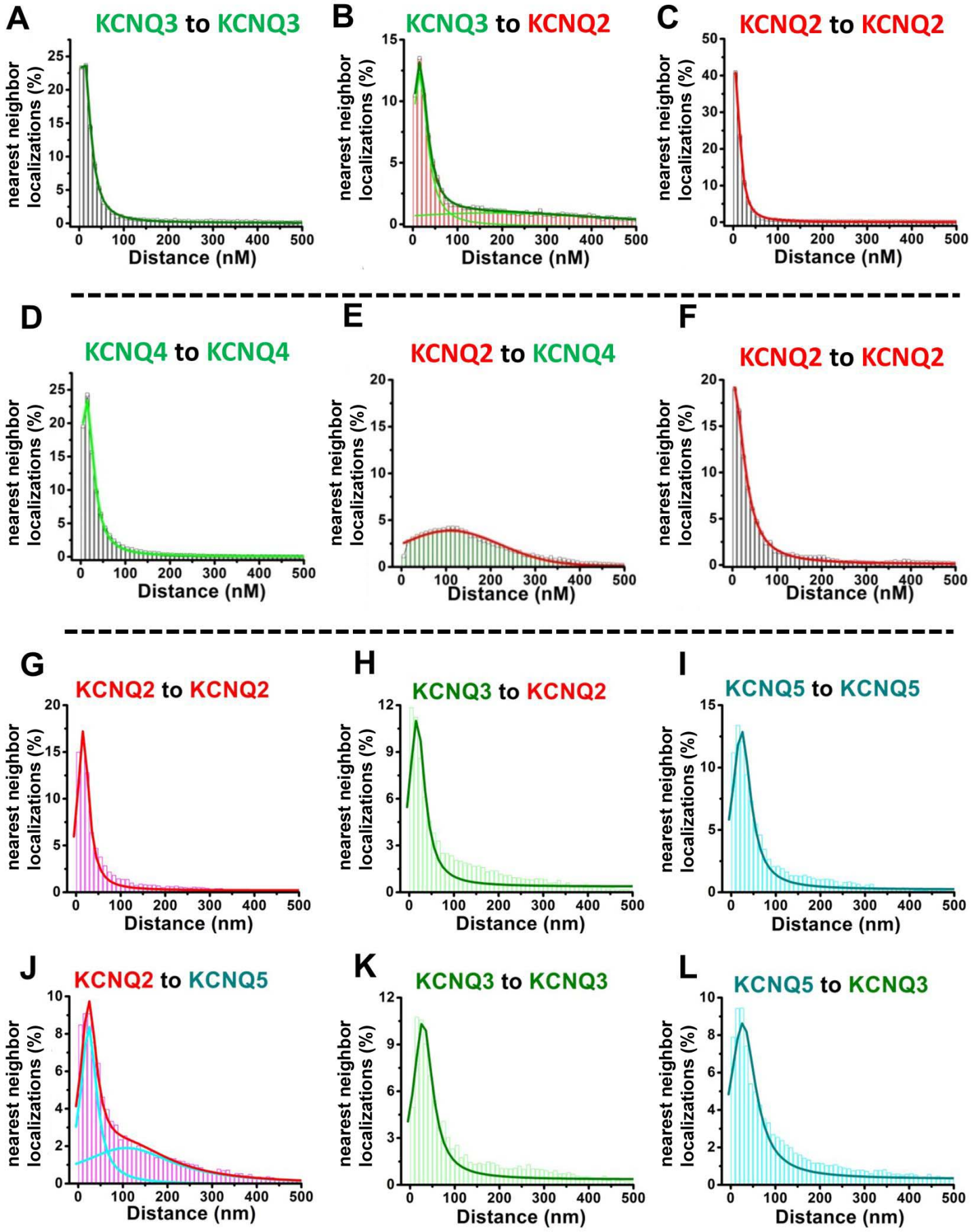


**Figure S2. Related to Figure 1. Nearest neighbor analysis for STORM images of Fig. 1.**

Figure S2 continued. For CHO cells co-transfected with KCNQ2+KCNQ3 (in **Fig.1A)**, plotted as histograms of percentage of molecules vs closest distance of nearest KCNQ3 molecule for each KCNQ3 molecule **(A)**, nearest KCNQ3 molecule for each KCNQ2 molecule **(B)**, and nearest KCNQ2 molecule for each KCNQ2 molecule **(C)**. For CHO cells co-transfected with KCNQ2+myc-tagged KCNQ4 (in **Fig.1B)**, plotted as histograms of percentage of molecules vs closest distance of nearest KCNQ4 molecule for each KCNQ4 molecule **(D)**, nearest KCNQ2 molecule for each KCNQ4 molecule **(E)**, and nearest KCNQ2 molecule for each KCNQ2 molecule **(F)**. For CHO cells co-transfected with KCNQ2+KCNQ3+myc-tagged KCNQ5 (in **Fig.1F)**, plotted as histograms of percentage of molecules vs closest distance of nearest KCNQ2 molecule for each KCNQ2 molecule **(G)**, nearest KCNQ3 molecule for each KCNQ2 molecule **(H)**, and nearest KCNQ5 molecule for each KCNQ5 molecule **(I)**, nearest KCNQ2 molecule for each KCNQ5 molecule **(J)**, nearest KCNQ3 molecule for each KCNQ3 molecule **(K)**, and nearest KCNQ5 molecule for each KCNQ3 molecule **(L).**

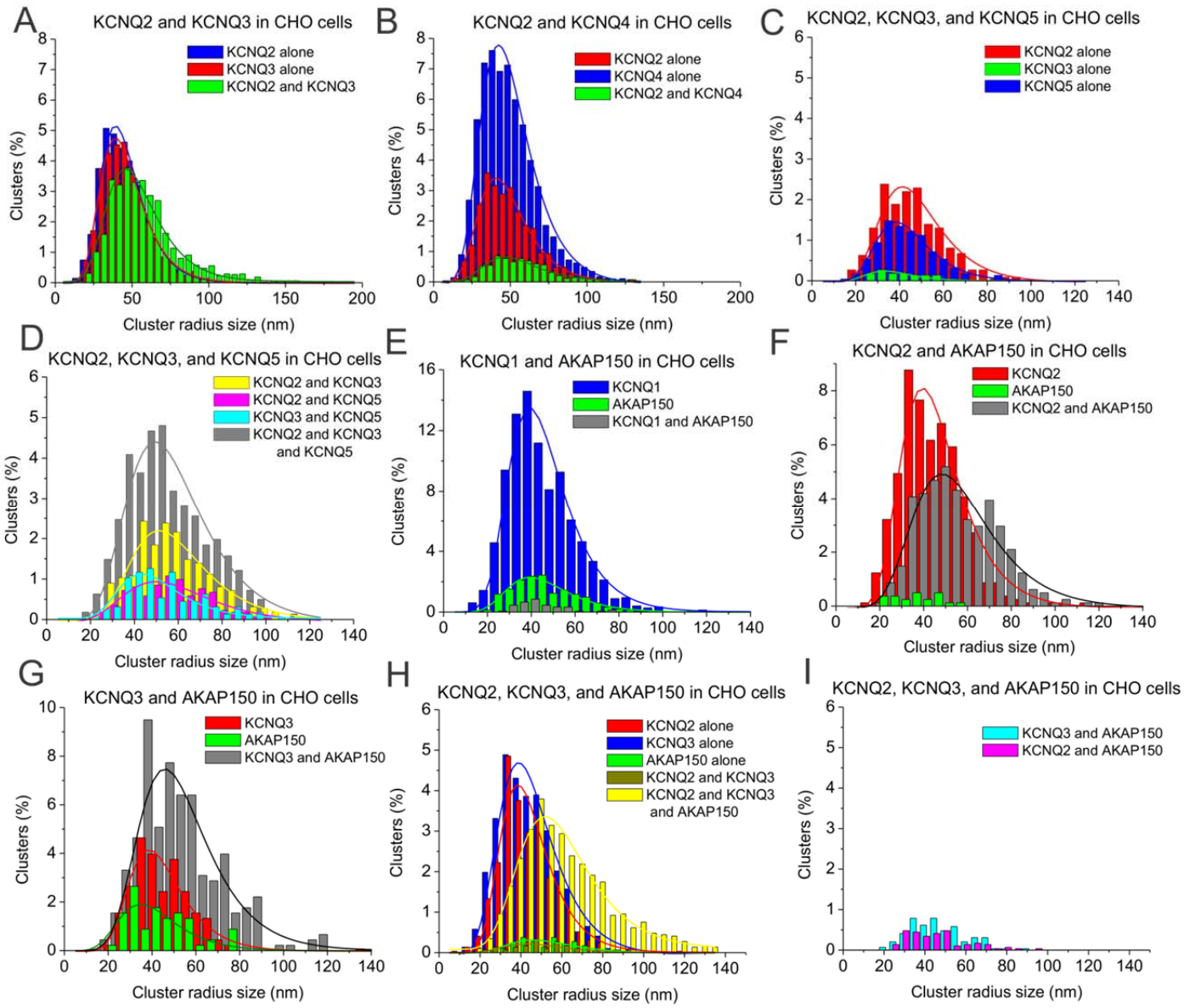


**Figure S3. Related to Figures 1 and 2. Cluster distribution of STORM localizations of KCNQ channels and AKAP150 in CHO cells.**

Histograms of cluster radius size (nm) of labeling for **(A)** KCNQ2 and KCNQ3 related to Figure 1A and 1D, **(B)** KCNQ2 and KCNQ4 related to Figure 1B and 1E, **(C,D)** KCNQ2, KCNQ3, and KCNQ5 related to Figure 1F-I. **(E)** KCNQ1 and AKAP150 related to Figure 2A, **(F)** KCNQ2 and AKAP150 related to Figure 2B, **(G)** KCNQ3 and AKAP150 related to Figure 2C, and **(H,I)** KCNQ2, KCNQ3, and AKAP150 related to Figure 2D.

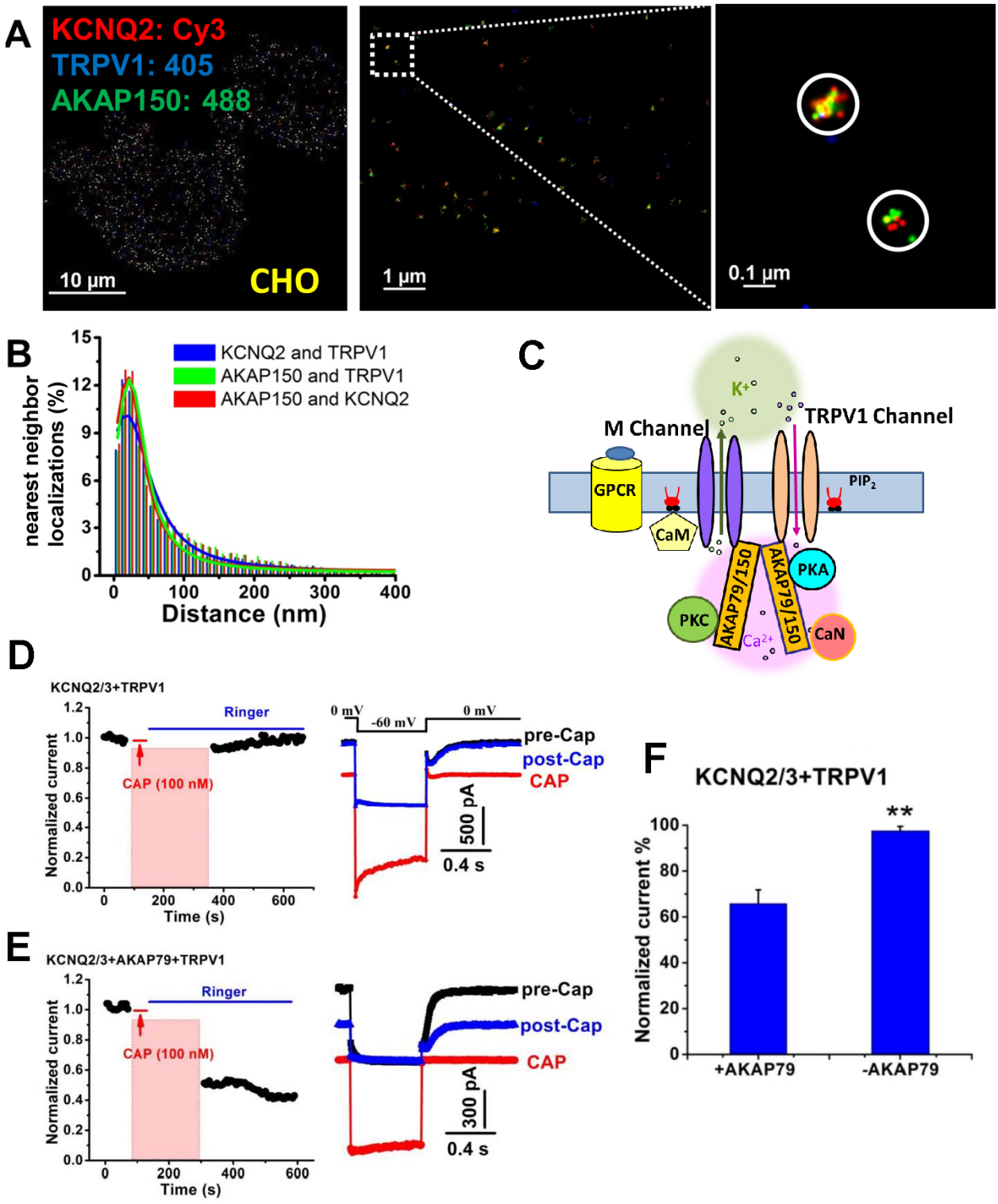


**Figure S4. Related to Figure 5. AKAP79/150-anchored M-channels and TRPV1 are physically and functionally coupled as larger multi-channel super-complexes.**

**(A)** Triple-color STORM images show AKAP150-mediated multi-channel complexes containing KCNQ2 and TRPV1 channels from CHO cells co-transfected with AKAP150, KCNQ2, and TRPV1. Cells were co-immunostained with rabbit anti-KCNQ2, GP anti-TRPV1 and, goat anti-AKAP150 antibodies, and secondaries conjugated with the indicated dye pairs. **(B)** Histogram distribution of STORM nearest-neighbor analysis are shown for AKAP150 and TRPV1, KCNQ2 and TRPV1, and AKAP150 and KCNQ2 from these cells, indicating intimate association of KCNQ2 and TRPV1 channels and AKAP150. n=4 cells**. (C)** Proposed model for multi-channel super-complexes from two distinct ion channels organized by an AKAP79/150 dimer. **D)** Plotted are normalized KCNQ2/3 current amplitudes from CHO cells transfected with KCNQ2+KCNQ3 and TRPV1, where activation of TRPV1 current has no effect on KCNQ2/3-current amplitude. **(E)**

Plotted are normalized KCNQ2/3 current amplitudes CHO cells transfected with KCNQ2+KCNQ3 and TRPV1 with co-transfection of AKAP79, where activation of TRPV1 current suppresses KCNQ2/3 current amplitude. Capsaicin (Cap) was applied during the periods shown by the red bars and representative current traces are shown on the right. Since KCNQ2/3 current cannot be quantified during activation of TRPV1 current, those regions of the amplitudes plots have been blanked out. **(F)** Bars summarize the normalized current amplitudes after Cap application for the groups of cells from E-F. n=9 and 9 cells**.** **$p<0.01$.

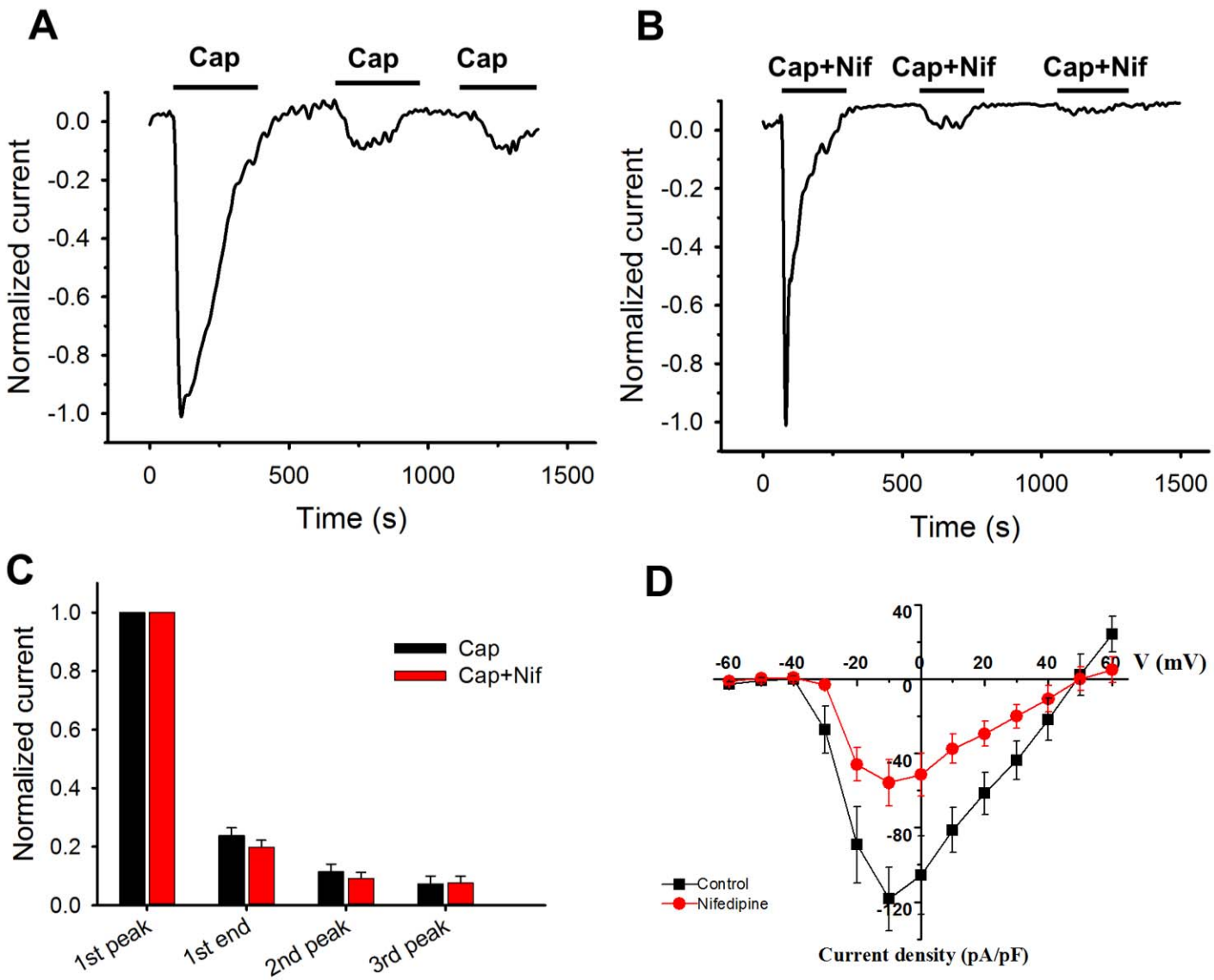


**Figure S5. Related to Figure 9. Nifedipine itself has no effect on desensitization of TRPV1 current.**
**(A)** In CHO cells transfected with only TRPV1, TRPV1 current recorded shows profound acute desensitization and tachyphalaxis upon three times application of capsaicin (Cap, 1 μM). **(B)** Both acute desensitization and tachyphalaxis are not affected when Nif (10 μM) is co-applied with Cap to block L-type $Ca^{2+}$ channels. **(C)** Bars summarize the normalized current amplitudes for the groups of cells from A-B. n=3 and 3 cells. **(D)** Current/voltage relationships of $Ca^{2+}$ currents in NG neurons in control conditions in the presence of nifedipine (10 μM), showing the voltage-dependence of the Nif-sensitive (L-type) channels in these neurons.

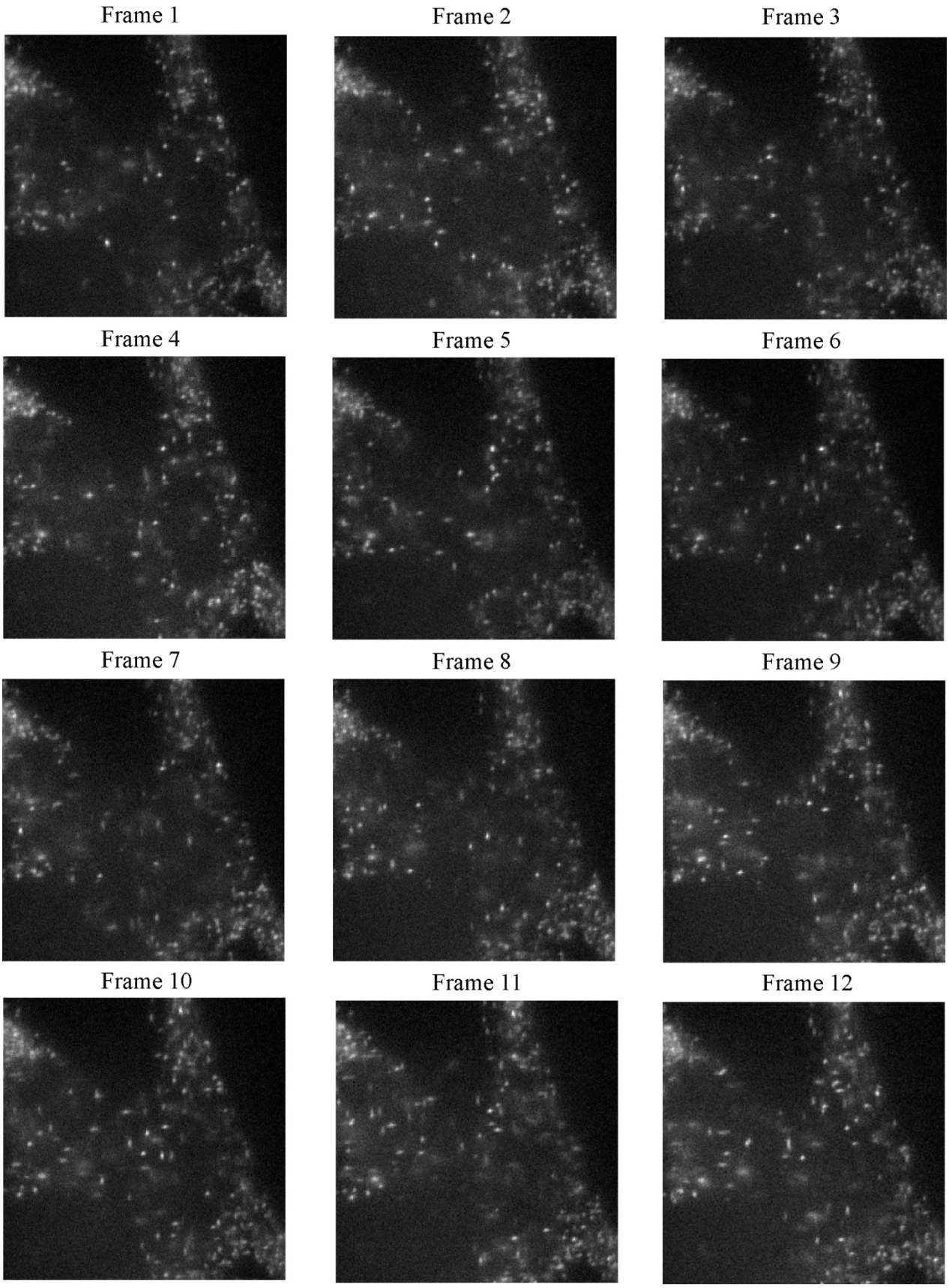


**Figure S6. Related to Figure 3. Representative sequential frames of raw STORM image acquisition of Alexa647 reporter fluorescence.** STORM acquisitions from a sensory neuron depicted in Figure 3A. Each frame in sequence is a 16 ms capture with the Alexa647 laser line, directly preceded by a single 16 ms excitation pulse of the 405 laser line.

**Table S1. Related to Figures 1 and 2. Detailed information about the fitted curves for STORM images in Figure 1 and 2.**

| CHO cells | Peak # | Peak Center (nm) | Peak Width (nm) | Peak Height |
|---|---|---|---|---|
| **KCNQ2 +KCNQ3** | | Lateral localization accuracy of 5.5 ± 1.7 nm | | |
| KCNQ3 to KCNQ3 | 1 | 10.2 ± 0.1 | 34.9 ± 0.3 | 25.4 |
| KCNQ3 to KCNQ2 | 1 | 15.3 ± 0.2 | 41.3 ± 0.8 | 12.4 |
| | 2 | 171 ± 24.0 | 664 ± 89.0 | 1.1 |
| KCNQ2 to KCNQ2 | 1 | 5.0 ± 0.1 | 23.4 ± 0.2 | 40.8 |
| KCNQ2 to KCNQ3 | 1 | 16.1 ± 0.2 | 32.8 ± 0.7 | 20.1 |
| | 2 | 103.7 ± 117.2 | 709.0 ± 324.9 | 0.7 |
| **KCNQ2 +KCNQ4** | | Lateral localization accuracy of 4.5 ± 0.8 nm | | |
| KCNQ4 to KCNQ4 | 1 | 13.0 ± 0.2 | 37.4 ± 0.6 | 23.6 |
| KCNQ4 to KCNQ2 | 1 | 139.0 ± 2.3 | 234.2 ± 5.5 | 3.5 |
| KCNQ2 to KCNQ2 | 1 | 2.6 ± 0.6 | 57.3 ± 0.9 | 19.2 |
| KCNQ2 to KCNQ4 | 1 | 109.2 ± 3.0 | 223.6 ± 6.9 | 3.8 |
| **KCNQ2 +KCNQ3+KCNQ5** | | Lateral localization accuracy of 8.0 ± 2.9 nm | | |
| KCNQ5 to KCNQ5 | 1 | 23.0 ± 1.1 | 49.7 ± 3.7 | 12.8 |
| KCNQ5 to KCNQ3 | 1 | 26.9 ± 1.9 | 69.6 ± 6.4 | 8.3 |
| KCNQ5 to KCNQ2 | 1 | 18.7 ± 1.0 | 30.4 ± 4.9 | 6.2 |
| | 2 | 110.3 ± 24.7 | 333.6 ± 60.9 | 2.6 |
| KCNQ3 to KCNQ3 | 1 | 28.9 ± 1.2 | 51.5 ± 4.0 | 10.2 |
| KCNQ3 to KCNQ5 | 1 | 23.8 ± 1.6 | 60.2 ± 5.4 | 9.6 |
| KCNQ3 to KCNQ2 | 1 | 17.2 ± 1.4 | 42.3 ± 4.4 | 10.7 |
| KCNQ2 to KCNQ2 | 1 | 16.0 ± 0.7 | 30.0 ± 2.0 | 17.1 |
| KCNQ2 to KCNQ3 | 1 | 23.0 ± 1.4 | 54.0 ± 4.6 | 9.9 |
| KCNQ2 to KCNQ5 | 1 | 23.3 ± 1.1 | 42.8 ± 5.9 | 8.5 |
| | 2 | 108.4 ± 36.7 | 256.3 ± 76.9 | 1.9 |
| **KCNQ1-AKAP150** | 1 | 119.0 ± 6.8 | 323.4 ± 14.7 | 2.9 |
| | | Lateral localization accuracy of 5.1 ± 1.3 nm | | |
| **KCNQ2-AKAP150** | 1 | 13.7 ± 0.9 | 63.2 ± 2.4 | 12.4 |
| | | Lateral localization accuracy of 6.1 ± 1.5 nm | | |
| **KCNQ3-AKAP150** | 1 | 33.3 ± 2.3 | 122.3 ± 6.9 | 7.7 |
| | | Lateral localization accuracy of 7.2 ± 2.3 nm | | |
| **KCNQ2 + KCNQ3 + AKAP150** | | Lateral localization accuracy of 8.3 ± 2.5 nm | | |
| KCNQ3 to AKAP150 | 1 | 19.5 ± 0.7 | 58.8 ± 2.1 | 11.6 |
| KCNQ2 to AKAP150 | 1 | 19.6 ± 0.6 | 51.7 ± 2.0 | 12.7 |
| KCNQ2 to KCNQ3 | 1 | 18.7 ± 0.5 | 52.5 ± 1.7 | 12.7 |

**Table S2. Related to Figures 3 and 4. Detailed information about the fitted curves for STORM images in Figure 3, 4, and S3.**

| | Peak # | Peak Center (nm) | | | Peak Width (nm) | | | Peak Height |
|---|---|---|---|---|---|---|---|---|
| **SCG neurons** | | | | | | | | |
| **KCNQ2 +KCNQ3+AKAP150** | | Lateral localization accuracy of 6.7 ± 2.3 nm | | | | | | |
| KCNQ3 to AKAP150 | 1 | 22.6 | ± | 1.0 | 73.6 | ± | 3.0 | 11.9 |
| KCNQ2 to AKAP150 | 1 | 22.1 | ± | 1.2 | 77.0 | ± | 3.5 | 11.5 |
| KCNQ2 to KCNQ3 | 1 | 22.7 | ± | 1.1 | 73.1 | ± | 3.3 | 11.8 |
| | | Lateral localization accuracy of 5.6 ± 1.6 nm | | | | | | |
| **AKAP150 to M1 receptor** | 1 | 13.7 | ± | 0.8 | 25.9 | ± | 2.3 | 28.5 |
| | | Lateral localization accuracy of 5.8 ± 1.7 nm | | | | | | |
| **AKAP150 to B2 receptor** | 1 | 115.2 | ± | 1.2 | 121 | ± | 5 | 7.0 |
| **CHO cells** | | | | | | | | |
| **KCNQ2 + M1 receptor+AKAP150** | | Lateral localization accuracy of 6.1 ± 1.5 nm | | | | | | |
| KCNQ2 to AKAP150 | 1 | 12.6 | ± | 0.3 | 44.4 | ± | 0.9 | 18.4 |
| KCNQ2 to M1 receptor | 1 | 26.6 | ± | 0.5 | 50.8 | ± | 3.4 | 6.8 |
| | 2 | 91.7 | ± | 42.6 | 485 | ± | 69 | 1.8 |
| AKAP150 to M1 receptor | 1 | 24.8 | ± | 0.5 | 47.3 | ± | 3.4 | 8.2 |
| | 2 | 92.0 | ± | 42.4 | 401 | ± | 68 | 1.8 |
| **KCNQ2 + B2 receptor+AKAP150** | | Lateral localization accuracy of 5.4 ± 1.5 nm | | | | | | |
| KCNQ2 to AKAP150 | 1 | 22.8 | ± | 1.3 | 65.1 | ± | 4.1 | 10.0 |
| KCNQ2 to B2 receptor | 1 | 144.6 | ± | 3.7 | 314 | ± | 9 | 2.9 |
| AKAP150 to B2 receptor | 1 | 126.9 | ± | 2.0 | 220 | ± | 5 | 3.3 |
| **KCNQ2 + TRPV1+AKAP150** | | Lateral localization accuracy of 7.2 ± 1.8 nm | | | | | | |
| KCNQ2 to TRPV1 | 1 | 23.4 | ± | 0.6 | 56.0 | ± | 2.0 | 12.2 |
| AKAP150 to TRPV1 | 1 | 20.3 | ± | 0.9 | 55.6 | ± | 2.8 | 12.3 |
| AKAP150 to KCNQ2 | 1 | 18.8 | ± | 1.6 | 83.6 | ± | 4.3 | 10.0 |

**Table S3. Related to Figures 5-7. Detailed information about the fitted curves for STORM images in Figure 5, 6, and 7.**

| | Peak # | Peak Center (nm) | Peak Width (nm) | Peak Height |
|---|---|---|---|---|
| **NG neurons** | | | | |
| **AKAP150+/+** | | | | |
| | | Lateral localization accuracy of 8.7 ± 2.6 nm | | |
| **Cav1.2 to AKAP150** | 1 | 13.3 ± 0.6 | 26.7 ± 1.8 | 22.2 |
| | | Lateral localization accuracy of 7.6 ± 4.2 nm | | |
| **TRPV1 to AKAP150** | 1 | 18.4 ± 0.6 | 52.1 ± 1.7 | 17.1 |
| **KCNQ2 + TRPV1+AKAP150** | | Lateral localization accuracy of 6.3 ± 2.5 nm | | |
| KCNQ2 to TRPV1 | 1 | 24.3 ± 1.6 | 72.8 ± 5.4 | 11.5 |
| AKAP150 to TRPV1 | 1 | 18.5 ± 0.8 | 51.3 ± 2.6 | 17.1 |
| AKAP150 to KCNQ2 | 1 | 19.4 ± 1.1 | 62.1 ± 3.6 | 14.0 |
| **TRPV1 + Cav1.2 +AKAP150** | | Lateral localization accuracy of 9.8 ± 3.6 nm | | |
| TRPV1 to Cav1.2 | 1 | 24.8 ± 1.9 | 101 ± 6 | 9.4 |
| AKAP150 to TRPV1 | 1 | 20.5 ± 1.2 | 74.4 ± 3.6 | 12.3 |
| AKAP150 to Cav1.2 | 1 | 13.5 ± 1.4 | 58.8 ± 3.7 | 13.7 |
| **AKAP150-/-** | | | | |
| | | Lateral localization accuracy of 7.3 ± 2.5 nm | | |
| **KCNQ2 to TRPV1** | 1 | 68.5 ± 0.8 | 99.6 ± 3.0 | 8.8 |
| | | Lateral localization accuracy of 6.5 ± 2.6 nm | | |
| **TRPV1 to Cav1.2** | 1 | 73.1 ± 1.5 | 161 ± 6 | 5.5 |

**Table S4. Related to Figures 1-8 and S3. Mean percentages of STORM cluster distributions detected by DBSCAN.**

| | | | | | | | |
|---|---|---|---|---|---|---|---|
| **CHO cells** | | | | | | | |
| **KCNQ2/KCNQ3** | KCNQ2 | KCNQ3 | KCNQ3+ KCNQ2 | | | | |
| | 33.4 ± 2.8% | 33.4 ± 3.3% | 33.2 ± 5.7% | | | | |
| **KCNQ2/KCNQ4** | KCNQ2 | KCNQ4 | KCNQ2+ KCNQ4 | | | | |
| | 27.1 ± 0.03% | 61.8 ± 6.0% | 11.1 ± 5.7% | | | | |
| **KCNQ2/KCNQ3/ KCNQ5** | KCNQ2 | KCNQ3 | KCNQ5 | KCNQ2+ KCNQ3 | KCNQ2+ KCNQ5 | KCNQ3+ KCNQ5 | KCNQ2+KCNQ3 +KCNQ5 |
| | 16.1 ± 3.3% | 1.1 ± 0.2% | 8.7 ± 1.0% | 18.3 ± 0.7% | 8.3 ± 0.6% | 8.6 ± 0.8% | 38.9 ± 5.2% |
| **KCNQ1/AKAP150** | KCNQ1 | AKAP150 | KCNQ1+ AKAP150 | | | | |
| | 81.1 ± 3.3% | 15.0 ± 2.7% | 3.9 ± 1.4% | | | | |
| **KCNQ2/AKAP150** | KCNQ2 | AKAP150 | KCNQ2+ AKAP150 | | | | |
| | 45.0 ± 9.1% | 1.4 ± 0.05% | 53.6 ± 8.5% | | | | |
| **KCNQ3/AKAP150** | KCNQ3 | AKAP150 | KCNQ3+ AKAP150 | | | | |
| | 23.6 ± 3.6% | 14.3 ± 3.4% | 62.1 ± 0.1% | | | | |
| **KCNQ2/KCNQ3/ AKAP150** | KCNQ2 | AKAP150 | KCNQ3 | KCNQ2+ KCNQ3 | KCNQ2+ AKAP150 | KCNQ3+ AKAP150 | KCNQ2+KCNQ3 +AKAP150 |
| | 24.0 ± 1.6% | 2.0 ± 0.04% | 32.1 ± 1.3% | 1.7 ± 0.05% | 3.9 ± 1.1% | 2.7 ± 0.03% | 33.6 ± 3.8% |
| **$M_1$R/AKAP150/ KCNQ2** | $M_1$R | AKAP150 | KCNQ2 | $M_1$R+ AKAP150 | $M_1$R+ KCNQ2 | KCNQ2+ AKAP150 | $M_1$R+AKAP150 +KCNQ2 |
| | 38.5 ± 4.4% | 3.6 ± 0.02% | 29.4 ± 5.3% | 4.2 ± 0.04% | 1.4 ± 0.02% | 10.2 ± 1.7% | 12.8 ± 2.9% |
| **$B_2$R/AKAP150/ KCNQ2** | $B_2$R | AKAP150 | KCNQ2 | $B_2$R+ AKAP150 | $B_2$R+ KCNQ2 | KCNQ2+ AKAP150 | $B_2$R+AKAP150 +KCNQ2 |
| | 32.9 ± 4.8% | 7.0 ± 1.5% | 27.1 ± 5.6% | 2.3 ± 0.03% | 0.08 ± 0.02% | 24.8 ± 2.5% | 5.2 ± 0.09% |
| **SCG neurons** | | | | | | | |
| **KCNQ2/KCNQ3/ AKAP150** | KCNQ2 | AKAP150 | KCNQ3 | KCNQ2+ KCNQ3 | KCNQ2+ AKAP150 | KCNQ3+ AKAP150 | KCNQ2+KCNQ3 +AKAP150 |
| | 18.7 ± 0.9% | 1.7 ± 0.4% | 37.1 ± 1.5% | 1.6 ± 0.4% | 3.3 ± 0.9% | 3.0 ± 1.1% | 34.5 ± 2.4% |
| **$M_1$R/AKAP150** | $M_1$R | AKAP150 | $M_1$R+ AKAP150 | | | | |
| | 14.3 ± 2.6% | 1.4 ± 0.3% | 84.2 ± 2.7% | | | | |
| **NG neurons (WT)** | | | | | | | |
| **TRPV1/AKAP150** | TRPV1 | AKAP150 | TRPV1+ AKAP150 | | | | |
| | 34.0 ± 0.1% | 16.9 ± 5.8% | 49.0 ± 5.4% | | | | |
| **$Ca_v$1.2/AKAP150** | $Ca_v$1.2 | AKAP150 | $Ca_v$1.2+ AKAP150 | | | | |
| | 17.9 ± 4.0% | 1.6 ± 0.03% | 80.5 ± 4.0% | | | | |
| **TRPV1/AKAP150/ KCNQ2** | TRPV1 | AKAP150 | KCNQ2 | TRPV1+ AKAP150 | TRPV1+ KCNQ2 | KCNQ2+ AKAP150 | TRPV1+KCNQ2 +AKAP150 |
| | 8.4 ± 1.2% | 1.0 ± 0.02% | 4.3 ± 0.06% | 3.9 ± 1.1% | 3.8 ± 1.0% | 36.9 ± 3.1% | 41.7 ± 3.5% |
| **TRPV1/AKAP150/ $Ca_v$1.2** | TRPV1 | AKAP150 | $Ca_v$1.2 | TRPV1+ AKAP150 | TRPV1+ $Ca_v$1.2 | $Ca_v$1.2+ AKAP150 | TRPV1+$Ca_v$1.2 +AKAP150 |
| | 21.3 ± 3.4% | 0.08 ± 0.01% | 5.9 ± 0.09% | 9.1 ± 2.4% | 6.5 ± 1.7% | 10.0 ± 4.3% | 46.3 ± 4.9% |
| **NG neurons (AKAP150-/-)** | | | | | | | |
| **TRPV1/KCNQ2** | TRPV1 | KCNQ2 | TRPV1+ KCNQ2 | | | | |
| | 57.3 ± 8.6% | 37.5 ± 8.7% | 5.2 ± 0.2% | | | | |
| **TRPV1/ $Ca_v$1.2** | TRPV1 | $Ca_v$1.2 | TRPV1+ $Ca_v$1.2 | | | | |
| | 80.0 ± 8.6% | 17.5 ± 7.6% | 2.5 ± 1.0% | | | | |

**All data values represent mean percentage of total clusters ± SEM. n = 4-8 cells per labeling group.**

**Table S5. Related to Figures 3 and 5-8. Mean cluster radius sizes of STORM-derived clusters detected by DBSCAN.**

| | | | | | | | |
|---|---|---|---|---|---|---|---|
| **SCG neurons** | | | | | | | |
| **KCNQ2/KCNQ3/ AKAP150** | KCNQ2 | AKAP150 | KCNQ3 | KCNQ2+ KCNQ3 | KCNQ2+ AKAP150 | KCNQ3+ AKAP150 | KCNQ2+KCNQ3 +AKAP150 |
| Cluster size (nm) | 41.5 ± 1.3 | 47.1 ± 1.5 | 42.8 ± 1.5 | 40.6 ± 1.2 | 41.4 ± 1.5 | 44.5 ± 1.6 | 61.4 ± 2.4 |
| β scale parameter | 13.0 | N/A | 11.7 | N/A | N/A | N/A | 15.8 |
| **$M_1$R/AKAP150** | $M_1$R | AKAP150 | $M_1$R+ AKAP150 | | | | |
| Cluster size (nm) | 39.0 ± 1.2 | 35.1 ± 2.9 | 62.2 ± 3.2 | | | | |
| β scale parameter | 12.4 | N/A | 18.9 | | | | |
| **AKAP150+/+ NG neurons** | | | | | | | |
| **TRPV1/AKAP150** | TRPV1 | AKAP150 | TRPV1+ AKAP150 | | | | |
| Cluster size (nm) | 47.4 ± 0.6 | 45.4 ± 3.1 | 65.3 ± 0.5 | | | | |
| β scale parameter | 12.8 | N/A | 20.4 | | | | |
| **$Ca_v$1.2/AKAP150** | AKAP150 | $Ca_v$1.2 | $Ca_v$1.2+ AKAP150 | | | | |
| Cluster size (nm) | 38.2 ± 3.1 | 45.3 ± 1.8 | 68.1 ± 5.0 | | | | |
| β scale parameter | N/A | 12.6 | 19.9 | | | | |
| **TRPV1/AKAP150/ KCNQ2** | TRPV1+ AKAP150 | TRPV1+ KCNQ2 | KCNQ2+ AKAP150 | TRPV1+ KCNQ2+ AKAP150 | | | |
| Cluster size (nm) | 51.0 ± 2.2 | 53.5 ± 1.8 | 63.7 ± 5.0 | 66.4 ± 4.4 | | | |
| β scale parameter | 13.6 | 12.9 | 17.5 | 19.0 | | | |
| **TRPV1/AKAP150/ $Ca_v$1.2** | TRPV1+ AKAP150 | TRPV1+ $Ca_v$1.2 | $Ca_v$1.2+ AKAP150 | TRPV1+ $Ca_v$1.2+ AKAP150 | | | |
| Cluster size (nm) | 64.4 ± 2.8 | 61.8 ± 2.7 | 56.9 ± 3.7 | 79.2 ± 4.9 | | | |
| β scale parameter | 16.1 | 18.2 | 15.3 | 27.7 | | | |
| **AKAP150-/- NG neurons** | | | | | | | |
| **TRPV1/KCNQ2** | TRPV1 | KCNQ2 | TRPV1+ KCNQ2 | | | | |
| Cluster size (nm) | 65.3 ± 2.1 | 61.8 ± 1.6 | 53.3 ± 2.0 | | | | |
| β scale parameter | 19.3 | 19.6 | N/A | | | | |
| **TRPV1/$Ca_v$1.2** | TRPV1 | $Ca_v$1.2 | TRPV1+ $Ca_v$1.2 | | | | |
| Cluster size (nm) | 64.5 ± 3.8 | 53.4 ± 2.2 | 43.4 ± 5.3 | | | | |
| β scale parameter | 19.7 | 15.2 | N/A | | | | |

**Cluster radius size (nm) represented by mean ± SEM. n = 4-8 cells per labeling group. The β continuous scale parameter was derived from the combined probability distribution function of all detected clusters of each category. N/A indicates cluster distributions that are under the noise threshold, in which a distribution function could not be reliably fit ($R^2 < 0.95$).**

**Table S6. Related to Figures 3 and 5-8. Mean number of localizations per cluster from STORM-derived clusters detected by DBSCAN.**

| | | | | | | | |
|---|---|---|---|---|---|---|---|
| **SCG neurons** | | | | | | | |
| **KCNQ2/KCNQ3/ AKAP150** | KCNQ2 | AKAP150 | KCNQ3 | KCNQ2+ KCNQ3 | KCNQ2+ AKAP150 | KCNQ3+ AKAP150 | KCNQ2+KCNQ3 +AKAP150 |
| Localizations | 9.4 ± 0.5 | 10.0 ± 0.3 ( < 2% of clusters) | 10.4 ± 0.4 | 7.8 ± 0.4 ( < 2% of clusters) | 8.7 ± 0.6 | 8.3 ± 0.6 | 13.4 ± 0.9 |
| **$M_1$R/AKAP150** | $M_1$R | AKAP150 | $M_1$R+ AKAP150 | | | | |
| Localizations | 8.4 ± 0.3 | 7.8 ± 0.5 | 22.1 ± 2.4 | | | | |
| **AKAP150+/+ NG neurons** | | | | | | | |
| **TRPV1/AKAP150** | TRPV1 | AKAP150 | TRPV1+ AKAP150 | | | | |
| Localizations | 11.4 ± 0.5 | 10.6 ± 0.7 | 17.6 ± 0.3 | | | | |
| Localizations>2*SD | | | **33.8 ± 0.4** | | | | |
| **$Ca_v1.2$/AKAP150** | $Ca_v1.2$ | AKAP150[1] | $Ca_v1.2$+ AKAP150 | | | | |
| Localizations | 9.0 ± 0.3 | 7.2 ± 0.2 | 27.0 ± 2.5* | | | | |
| Localizations>2*SD | | | **74.8 ± 3.3*** | | | | |
| **TRPV1/AKAP150/ KCNQ2** | TRPV1 | AKAP150[1] | KCNQ2 | TRPV1+ AKAP150 | TRPV1+ KCNQ2 | KCNQ2+ AKAP150 | TRPV1+ KCNQ2+ AKAP150 |
| Localizations | 15.1 ± 4.2 | 10.0 ± 1.6 | 8.0 ± 0.2 | 13.9 ± 1.5 | 16.1 ± 3.3 | 22.5 ± 3.5 | 20.2 ± 3.6 |
| Localizations>2*SD | | | | | | | **62.3 ± 4.4** |
| **TRPV1/AKAP150/ $Ca_v1.2$** | TRPV1 | AKAP150[1] | $Ca_v1.2$ | TRPV1+ AKAP150 | TRPV1+ $Ca_v1.2$ | $Ca_v1.2$+ AKAP150 | TRPV1+ $Ca_v1.2$+ AKAP150 |
| Localizations | 12.3 ± 0.3 | 8.4 ± 0.5 | 10.7 ± 0.6 | 17.2 ± 1.8 | 15.2 ± 1.7 | 15.8 ± 1.4 | 29.4 ± 2.0[#] |
| Localizations>2*SD | | | | | | | **77.5 ± 3.7**[#] |

* $p < 0.05$ vs. TRPV1 + AKAP150

[#] $p < 0.05$ vs. TRPV1 + KCNQ2 + AKAP150

Localizations > 2 *SD denotes clusters containing number of localizations that contained greater than 2 standard deviations from the mean value of the population.

[1] The number of AKAP150 clusters in these experiments is minimal (between 0.08 – 1.6% of total clusters)